



1

2

3

4

5

6

7 **Estimating Interception from Near-Surface Soil Moisture Response**

8

9

10

11

12

13

14 Subodh Acharya^{1*}, Daniel McLaughlin², David Kaplan³, and Matthew J. Cohen¹

15

16

17

18 1 – School of Forest Resources and Conservation, University of Florida, Gainesville FL

19 2 – Department of Forest Resources and Conservation, Virginia Tech, Blacksburg, VA

20 3 – Environmental Engineering Sciences Department, University of Florida, Gainesville FL

21

22 * – Corresponding Author

23



24

Abstract

25 Interception is the storage and subsequent evaporation of rainfall by above-ground
26 structures, including canopy and groundcover vegetation and surface litter. Accurately
27 quantifying interception is critical for understanding how ecosystems partition incoming
28 precipitation, but it is difficult and costly to measure, leading most studies to rely on modeled
29 interception estimates. Moreover, forest interception estimates typically focus only on canopy
30 storage, despite the potential for substantial interception by groundcover vegetation and surface
31 litter. In this study, we developed an approach to quantify “total” interception losses (i.e.,
32 including forest canopy, understory, and surface litter layers) using measurements of shallow soil
33 moisture dynamics during rainfall events. Across 36 pine and mixed forest stands in Florida
34 (USA), we used soil moisture and rainfall data to estimate the interception storage capacity (β_s),
35 a parameter required to estimate total annual interception losses (I_a) relative to rainfall (R).
36 Estimated values for β_s (mean $\beta_s = 0.30$ cm; $0.01 \leq \beta_s \leq 0.62$ cm) and I_a/R (mean $I_a/R = 0.14$;
37 $0.06 \leq I_a/R \leq 0.21$) were consistent with reported literature values for these ecosystems and were
38 significantly predicted by forest structural attributes (leaf area index and percent groundcover),
39 as well as other site variables (e.g., water table depth). The best-fit model was dominated by LAI
40 and explained nearly 80% of observed β_s variation. These results suggest that whole-forest
41 interception can be measured using a single near-surface soil moisture time series and highlight
42 the variability in interception losses across a single forest type, underscoring the need for
43 expanded empirical measurement. Potential cost savings and logistical advantages of this method
44 relative to conventional, labor-intensive interception measurements may improve empirical
45 estimation of this critical water budget element.

46



47

Introduction

48 Rainfall interception (I) is the fraction of incident rainfall stored by above-ground
49 ecosystem structures (i.e., vegetation and litter layers) and subsequently returned to the
50 atmosphere via evaporation (E), never reaching the soil surface and thus never directly
51 supporting transpiration (T) [Savenije, 2004]. Interception depends on climate and vegetation
52 characteristics and can be as high as 50% of gross rainfall [Gerrits *et al.*, 2007; 2010; Calder,
53 1990]. Despite being critical for accurate water budget enumeration [David *et al.*, 2005],
54 interception is often disregarded or lumped with evapotranspiration (ET) in hydrological models
55 [Savenije, 2004]. Recent work suggests interception uncertainty constrains efforts to partition ET
56 into T and E , impairing representation of water use and yield in terrestrial ecosystems [Wei *et al.*,
57 2017].

58 When interception is explicitly considered, it is typically empirically estimated or
59 modeled solely for the tree canopy. For example, direct measurements are often obtained from
60 differences between total rainfall and water that passes through the canopy to elevated above-
61 ground collectors (throughfall) plus water that runs down tree trunks (stemflow) during natural
62 [e.g., Bryant *et al.*, 2005, Ghimire *et al.*, 2012, 2016] or simulated [e.g., Guevara-Escobar *et al.*,
63 2007; Putuhena and Cordery, 1996] rainfall events. This method yields the rainfall fraction held
64 and subsequently lost by the canopy but ignores interception by understory vegetation and litter.
65 Alternatively, numerous empirical [e.g., Merriam, 1960], process-based [e.g., Rutter *et al.*, 1971,
66 1975; Gash, 1979, 1995, Liu, 1998], and stochastic [Calder, 1986] models are available for
67 estimating interception. As with direct measurements, most model applications consider only
68 canopy storage despite groundcover (both understory vegetation and litter layers) interception
69 that can exceed canopy values [Gerrits and Savenije, 2011; Putuhena and Cordery, 1996]. As



70 such, it seems likely that conventional measures and typical model applications underestimate
71 actual (i.e., “total”) interception.

72 New field approaches are needed to improve quantification of total interception and
73 refine the calibration and application of available models. A detailed review of available
74 interception models [Muzylo *et al.*, 2009] stresses the need for direct interception measurements
75 across forest types and hydroclimatic regions, but meeting this need will require substantial
76 methodological advances. Throughfall measurements yield direct and site-specific interception
77 estimates [e.g., Ghimire *et al.*, 2017; Bryant *et al.*, 2005], but they are difficult and costly to
78 implement even at the stand scale because of high spatial and temporal variability in vegetation
79 structure. Moreover, comprehensive measurements also require enumeration of spatially
80 heterogeneous stemflow, as well as interception storage by the understory and litter layers,
81 greatly exacerbating sampling complexity and cost [Lundberg *et al.*, 1997]. Empirical techniques
82 that estimate total interception, integrate across local spatial and temporal variation, and
83 minimize field installation complexity are clearly desirable.

84 Here we present a novel approach for estimating total (i.e., canopy, understory and litter)
85 interception using continuously logged, near-surface soil moisture. Prior to runoff generation,
86 infiltration is equivalent to rainfall minus total interception, and the response of near-surface soil
87 moisture during and directly following rain events can be used to inform interception parameters
88 and thus interception losses. Since soil moisture is relatively easy and economical to measure
89 continuously for extended periods, successful inference of interception from soil moisture time
90 series may greatly expand the temporal and spatial domains of empirical interception
91 measurements. As a proof-of-concept, we tested this simple interception estimation method in 36



92 forest plots spanning a wide range of conditions (e.g., tree density, composition, groundcover,
93 understory management, age, and hydrogeologic setting) across Florida (USA).

94

95 **Methods**

96 **Estimating Interception Storage Capacity from Soil Moisture Data**

97 During every rainfall event, a portion of the total precipitation (P) is temporarily stored in
98 the forest canopy and groundcover (hereafter referring to both live understory vegetation and
99 forest floor litter). We assume that infiltration (and thus any increase in soil moisture) begins
100 only after total interception storage, defined as the sum of canopy and groundcover storage, is
101 full. We further assume this stored water subsequently evaporates to meet atmospheric demand.
102 Calculating dynamic interception storage requires first determining the total storage capacity
103 (β_s), which is comprised of the storage capacities for the forest canopy (β_c) and groundcover (β_g)
104 (Fig. 1a).

105 To estimate β_s , we consider a population of individual rainfall events of varying depth
106 over a forest for which high frequency (i.e., 4 hr^{-1}) soil-moisture measurements are available
107 from near the soil surface. Soil moisture content (SMC) at the sensor changes only after rainfall
108 fills total interception storage, evaporative demands since rainfall onset are met, and there is
109 sufficient infiltration for the wetting-front to arrive at the sensor. Rainfall events large enough to
110 induce a soil moisture change (ΔSMC) are evident as a rainfall threshold in the relationship
111 between P and ΔSMC . An example time series of P and SMC (Fig. 1b) yields a P versus ΔSMC
112 relationship (Fig. 1c) with clear threshold behavior. There are multiple equations whose
113 functional forms allow for extraction of this threshold; here we express this relationship as:

$$114 \quad P = \frac{a}{(1+b \cdot \exp(-c \cdot \Delta SMC))} \quad (1)$$



115 where P is the total rainfall event depth, ΔSMC is the corresponding soil moisture change, and a ,
 116 b , and c are fitted parameters. Figure 2 illustrates this relationship and model fitting for observed
 117 SMC data from six plots at one of our study sites described below. The x-intercept of Eq. 1 (i.e.,
 118 where ΔSMC departs from zero) is given by:

$$119 \quad P_s = \frac{a}{(1+b)} \quad (2)$$

120 Empirically observed values of P_s represent the total rainfall required to saturate β_s , meet
 121 evaporative demands between storm onset and observed ΔSMC , and supply any infiltration
 122 required to induce soil moisture response once interception storage has been saturated. This
 123 equality can be expressed as:

$$124 \quad P_s = \beta_s + \int_0^T E dt + \int_t^T f dt = \beta_s + \int_0^t E dt + \int_t^T E dt + \int_t^T f dt \quad (3)$$

125 where T is the total time from rainfall onset until observed change in SMC (i.e., the wetting front
 126 arrival), t is the time when β_s is satisfied, and E and f are infiltration and evaporation rates,
 127 respectively. To connect this empirical observation to existing analytical frameworks (e.g., Gash
 128 1979), we adopt the term P_G , defined as the rainfall depth needed to saturate β_s and supply
 129 evaporative losses between rainfall onset ($t = 0$) and β_s saturation ($t = t$):

$$130 \quad P_G = \beta_s + \int_0^t E dt \quad (4)$$

131 Solving for β_s in Eq. 3 and substituting into Eq. 4 yields:

$$132 \quad P_G = P_s - \int_t^T E dt - \int_t^T f dt \quad (5)$$

133 Equation 5 may be simplified by assuming that average infiltration and evaporation rates apply
 134 during the relatively short period between t and T , such that:

$$135 \quad P_G = P_s - \bar{f}(T - t) - \bar{E}(T - t) \quad (6)$$



136 where \bar{f} is the average soil infiltration rate and \bar{E} is the average rate of evaporation from the
 137 forest surface (i.e., canopy, groundcover, and soil) during the time from t to T (see Gash 1979).
 138 The storage capacity β_s can now be calculated following Gash (1979) as:

$$139 \quad \beta_s = -P_G \frac{\bar{E}}{\bar{R}} \ln \left(1 - \frac{\bar{E}}{\bar{R}} \right) = \frac{-\bar{E} [P_s - (T-t)(\bar{f} + \bar{E})]}{\bar{R} \ln \left(1 - \frac{\bar{E}}{\bar{R}} \right)} \quad (7)$$

140 where \bar{R} is the rainfall rate and all other variables are as previously defined. In Eq. 5, \bar{E} is usually
 141 estimated using the Penman-Monteith equation [Monteith, 1965], setting canopy resistance to
 142 zero (e.g., Ghimire et al 2017).

143 A key challenge in applying Eq. 5, and thus for the overall approach, is quantifying
 144 infiltration, since the time, t , when P_G is satisfied is unknown. Moreover, the infiltration rate
 145 embedded in P_s is controlled by the rainfall rate (\bar{R}) and initial soil moisture content (θ_i). It is
 146 worth noting that shallower sensor depth placement would likely eliminate the need for this step
 147 (see Discussion). However, to overcome this limitation in our study, we used the 1-D unsaturated
 148 flow model HYDRUS-1D (Simunek et al., 1995) to simulate the time it takes for the wetting
 149 front to arrive (T_w) at the sensor under bare soil conditions across many combinations of \bar{R} and
 150 θ_i . As such, T_w represents the time required for a soil moisture pulse to reach the sensor once
 151 infiltration begins (i.e., after total interception capacity has been filled), which is $T - t$ in Eq. 7.
 152 For each simulation, T_w (signaled by the first change in SMC at sensor depth) was recorded and
 153 used to develop a statistical model of T_w as a function of \bar{R} and θ_i . We used plot-specific soil
 154 moisture retention parameters from Florida Soil Characterization Retrieval System
 155 (<https://soils.ifas.ufl.edu/flsoils/>) to develop these curves for our six sites, but simulations can be
 156 applied for any soil with known or estimated parameters.

157 Simulations revealed that T_w at a specific depth declined exponentially with increasing θ_i :

$$158 \quad T_w = ae^{-b\theta_i} \quad (8)$$



159 where a and b are fitting parameters. Moreover, the parameters a and b in Eq. (6) are well fitted
160 by a power function of \bar{R} :

$$161 \quad a = a_1 \bar{R}^{a_2}, b = b_1 \bar{R}^{b_2} \quad (9)$$

162 where a_1 and b_1 are fitting parameters. These relationships are illustrated in Fig. 3 for a loamy
163 sand across a range of \bar{R} and θ_i . The relationship between initial SMC and T_w is very strong for
164 small to moderate \bar{R} (< 3.0 cm/hr). At higher values of \bar{R} , T_w is smaller than the 15-minute
165 sampling resolution, and these events were excluded from our analysis (see below).

166 Assuming that \bar{f} equals \bar{R} over the initial infiltration period from t to T (robust for most
167 soils, see below), Eq. 7 can be modified to:

$$168 \quad \beta_s = \frac{-\dot{E}}{\dot{R}} \left[\frac{P_s - T_w(\dot{R} + \dot{E})}{\ln\left(1 - \frac{\dot{E}}{\dot{R}}\right)} \right] \quad (10)$$

169 This approach assumes no runoff or lateral soil-water flow near the top of the soil profile from
170 time t to T . Except for very fine soils under extremely high \bar{R} , this assumption generally holds
171 during early storm phases, before ponding occurs (Mein and Larsen, 1973). Moreover, since our
172 goal is to determine β_s , extreme storms can be omitted from the analysis when implementing
173 Eqs. 1-10, without compromising our estimates. Finally, we note that values of β_s from Eq. 10
174 represent combined interception from canopy and groundcover, but the method does not allow
175 for disaggregation of these two components.

176 **Calculating Interception Loss**

177 Interception storage and resulting interception loss for a given rain event are driven by
178 both antecedent rain (which fills storage) and evaporation (which depletes it). Instantaneous
179 available storage ranges from zero (saturated) to the maximum capacity (i.e., β_s which occurs
180 when the storage is empty). While discrete, event-based interception models [*Gash*, 1979, 1995;
181 *Liu*, 1998] have been widely applied to estimate interception, continuous models more accurately



182 represent time-varying dynamics in interception storage and losses. We adopted the continuous,
183 physically-based interception modeling framework of *Liu* [1998, 2001]:

$$184 \quad I = \beta_s(D_0 - D) + \int_0^T (1 - D)E dt \quad (11)$$

185 where I is interception, E is the evaporation rate from wetted surfaces, D_0 is the forest dryness
186 index at the beginning of a rain event, and D is the forest dryness index at time T . The dryness
187 index is calculated as:

$$188 \quad D = 1 - \frac{C}{\beta_s} \quad (12)$$

189 where C is “adherent storage” (i.e., water that does not drip to the ground) and is given by:

$$190 \quad C = \beta_s \left(1 - D_0 \exp\left(\frac{-(1-\tau)P}{\beta_s}\right) \right) \quad (13)$$

191 where τ is the free throughfall coefficient. Because our formulation of β_s in Eq. 10 incorporates
192 both canopy and groundcover components (i.e., negligible true throughfall), we approximated τ
193 in Eq. 13 as zero. For single storms or when sufficient time has passed to dry the canopy, D_0 is
194 assumed to be unity [*Liu* 2001]. Between rainfall events, water in interception storage evaporates
195 to meet atmospheric demand, until the dryness index, D reaches unity [*Liu* 1997]. The rate of
196 evaporation from wetted surfaces between rainfall events (E_s) is:

$$197 \quad E_s = E(1 - D_0) \exp\left(\frac{E}{\beta_s}\right) \quad (14)$$

198 A numerical version of Eq. 9 to calculate interception at each time step, t , is expressed as:

$$199 \quad I = \beta_s(D_{t-1} - D_t) + \frac{1}{2}[E_{t-1}(1 - D_{t-1}) + E_t(1 - D_t)] \quad (15)$$

200 Eq. 15 quantifies continuous and cumulative interception losses using precipitation and other
201 climate data (for E) along with β_s derived from soil moisture measurements and corresponding
202 meteorological data.



203 Study Area and Data

204 As part of a multi-year study quantifying forest water use under varying silvicultural
205 management, we instrumented six sites across Florida, each with six 2-ha plots spanning a wide
206 range of forest structural characteristics. Sites varied in hydroclimatic forcing (annual
207 precipitation range: 131 to 154 cm/yr and potential *ET* range: 127 to 158 cm/yr) and
208 hydrogeologic setting (shallow vs. deep groundwater table). Experimental plots within sites
209 varied in tree species, age, density, leaf area index (LAI), groundcover density (%GC), soil type,
210 and management history (Table 1). Each site contained a recent clear-cut plot, a mature pine
211 plantation plot, and a restored longleaf pine (*Pinus palustris*) plot; the three remaining plots at
212 each site included stands of slash pine (*Pinus elliottii*), sand pine (*Pinus clausa*), or loblolly pine
213 (*Pinus taeda*) subjected to varying silvicultural treatments (understory management, canopy
214 thinning, prescribed burning) and hardwood encroachment.

215 Within each plot, three banks of TDR sensors (CS655, Campbell Scientific, Logan, UT,
216 USA) were installed to measure soil moisture at multiple soil depths (Fig. 1a). Only data from
217 the top-most sensor (15 cm below the ground surface) were used in this study. Soil-moisture
218 sensor banks were located to capture representative variation in stand geometry (i.e., below the
219 tree canopy and within inter-canopy rows), and thus capture variation in surface soil moisture
220 response to rainfall events driven by forest canopy and groundcover differences. Within each
221 clear-cut plot at each site, meteorological data (rainfall, air temperature, relative humidity, solar
222 insolation, wind speed and direction) were measured using a weather station (GRSW100,
223 Campbell Scientific, Logan, UT; Fig. 4c) every 3 seconds and used to calculate hourly *E* by
224 setting the canopy resistance to zero [Ghimire *et al.*, 2017; Gash, 1995; Monteith, 1965].
225 Growing season forest canopy LAI (m² m⁻²) and groundcover (%) were measured at every 5-m



226 node within a 50 m x 50 m grid surrounding soil moisture measurement banks. LAI was
227 measured at a height of 1 m using a LI-COR LAI-2200 plant canopy analyzer, and %GC was
228 measured using a 1 m² quadrat.

229 To estimate β_s , mean ΔSMC values from the three surface sensors were calculated for all
230 rainfall events separated by at least 72 hours. Storm separation was necessary to ensure the
231 canopy and groundcover surfaces were mostly dry at the onset of each included rainfall event.
232 Rainfall events were binned into discrete classes by depth and plotted against mean ΔSMC to
233 empirically estimate P_s (e.g., Fig. 2). For each rainfall bin, mean θ_i , \bar{R} and \bar{E} were also calculated
234 to use in Eq. 10, which was then applied to calculate β_s . Subsequently, we developed generalized
235 linear models (GLMs) using forest canopy structure (site-mean LAI), mean groundcover (%
236 GC), hydrogeologic setting (shallow vs. deep groundwater table), and site as potential predictors,
237 along with their interactions, to statistically assess predictors of β_s estimates. Because models
238 differed in fitted parameter number, the best model was selected using the Akaike Information
239 Criteria (AIC; Akaike, 1974). Finally, we calculated cumulative annual interception loss (I_a) and
240 its proportion of total rainfall for each study plot using the mean β_s for each plot (across the 3
241 sensor banks), climate data from 2014 to 2016, and Eq. 15. All analyses were performed using R
242 statistical software [R Core Team, 2017].

243

244

Results

245 Total Storage Capacity (β_s)

246 The exponential function used to describe the P - ΔSMC relationship (Eq. 1) showed
247 strong agreement with observations at all sites and plots (overall $R^2 = 0.80$; $0.47 \leq R^2 \leq 0.97$;
248 Table 1) as illustrated for a single site in Fig. 2. This consistency across plots and sites suggests



249 that Eq. 1 is capable of adequately describing observed P - ΔSMC relationships, enabling
250 estimates of β_s across diverse hydroclimatic settings and forest structural variation. Estimates of
251 β_s ranged from 0.01 to 0.62 cm, with a mean of 0.30 cm. Plot-scale LAI was moderately
252 correlated with plot-mean β_s , describing roughly 32% of observed variation across plots (Fig.
253 4a). This relatively weak association may arise because LAI measurements only characterize
254 canopy cover, while β_s combines canopy and groundcover storage. The best GLM of β_s (Fig. 4b)
255 used %GC and an interaction term between site and LAI ($R^2 = 0.84$ and $AIC = 253.7$, Table 2).
256 The best GLM without site used LAI and hydrogeologic setting (shallow vs. deep water table)
257 but had reduced performance ($R^2 = 0.55$ and $AIC = 338.3$; Table 2).

258 **Annual Interception Losses (I_a)**

259 Despite having similar rainfall regimes (mean annual precipitation ranging from 131 to
260 154 cm yr⁻¹ across sites), mean annual interception losses (I_a) differed significantly both across
261 sites (one-way ANOVA $p < 0.001$) and among plots within sites (one-way ANOVA $p < 0.001$).
262 Estimates of I_a/P across all plots and sites ranged from 6 to 21% of annual rainfall (Table 1) and
263 were moderately, but significantly, correlated with mean LAI, explaining approximately 30% of
264 variation in I_a (Fig. 5a). Correlations among I_a/P and LAI were stronger for individual sites than
265 the global relationship ($0.51 \leq R^2 \leq 0.84$), except for site EF, where I_a losses were small and
266 similar across plots regardless of LAI (Fig. 5b; Table 1). This suggests that additional site-level
267 differences (e.g., hydroclimate, soils, geology) play a role in driving I_a , as expected following
268 from their effects on β_s described above.

269 **Discussion and Conclusions**

270 When combined with local rainfall data, near-surface soil moisture dynamics inherently
271 contain information about rainfall interception by above-ground structures. Using soil moisture



272 data, we developed and tested an analytical approach for estimating total interception storage
273 capacity (β_s) that includes canopy, understory, and groundcover vegetation, as well as any litter
274 on the forest floor. The range of β_s given by our analysis (mean $\beta_s = 0.30$ cm; $0.01 \leq \beta_s \leq 0.62$
275 cm) is close to, but generally higher than previously reported canopy storage capacity values for
276 similar pine forests (e.g., 0.17 to 0.20 cm for mature southeastern USA pine forests; Bryant et al.
277 2005).

278 An important distinction between our method and previous interception measurement
279 approaches is that the soil moisture-based method estimates composite rainfall interception of
280 not only the canopy, but also of the groundcover vegetation and forest floor litter. Rainfall
281 storage and subsequent evaporation from groundcover vegetation and litter layers can be as high,
282 or higher than, canopy storage in many forest landscapes [Putuhena and Cordery, 1996; Gerrits
283 et al., 2010]. For example, Li et al. [2017] found that the storage capacity of a pine forest floor in
284 China was between 0.3 and 0.5 cm, while maximum canopy storage was < 0.1 cm. Putuhena
285 and Cordery [1996] also estimated storage capacity of pine forest litter to be approximately 0.3
286 cm based on direct field measurements. Gerrits et al. [2007] found forest floor interception to be
287 34% of measured precipitation in a beech forest, while other studies have shown that interception
288 by litter can range from 8 to 18% of total rainfall [Gerrits et al., 2010; Tsiko et al., 2012; Miller
289 et al., 1990; Pathak et al., 1985; Kelliher et al., 1992]. A recent study using leaf wetness
290 observations [Acharya et al. 2017] found the storage capacity of eastern redcedar (*Juniperus*
291 *virginiana*) forest litter to range from 0.12 to as high as 1.12 cm, with forest litter intercepting
292 approximately 8% of gross rainfall over a six-month period. Given the composite nature of forest
293 interception storage and the range of storage capacities reported in these studies, the values we
294 report appear to be plausible, and consistent with the expected differences between canopy-only



295 and total interception storage. As such, our results support the general applicability of the soil
296 moisture-based approach for developing forest interception estimates across a wide range of
297 hydroclimatic and forest structural settings.

298 Interception losses vary spatially and temporally and are driven by both β_s and climatic
299 variation (i.e., P and E). Our approach represents storage dynamics by combining empirically
300 derived β_s estimates with climatic data using a previously developed continuous interception
301 model [Liu 1998, 2001]. Cumulative I_a estimates in this study ranged considerably (i.e., from 6%
302 to 21% of annual rainfall) across the 34 plots, which were characterized by variation in canopy
303 structure ($0.12 < \text{LAI} < 3.70$) and groundcover ($7.9 < \% \text{GC} < 86.2$). In comparison, interception
304 losses by pine forests reported in the literature (all of which report either canopy-only or
305 groundcover-only values, but not their composite) range from 12 to 49% of incoming rainfall
306 [Bryant *et al.*, 2005; Llorens *et al.*, 1997; Kelliher and Whitehead, 1992; Crockford and
307 Richardson, 1990]. Notably, most of the variation in this range is drive by climate rather than
308 forest structure, with the highest I_a values from more arid regions (e.g., Llorens *et al.* 1997).
309 Broad agreement between our results and literature I_a values supports the utility of our method
310 for estimating this difficult-to-measure component of the water budget. Additionally, the
311 magnitude and heterogeneity of our I_a estimates across a single forest type (southeastern US
312 pine) underscores the urgent need for empirical measurements of interception that incorporate
313 information on both canopy and groundcover storage in order to develop accurate water budgets.
314 This conclusion is further bolstered by the persistent importance of site-level statistical effects in
315 predicting β_s (and therefore I_a), even after accounting for forest structural attributes, which
316 suggests there are influential edaphic or structural attributes that we are not currently adequately
317 assessing.



318 Generally, estimated I_a losses in clear-cut plots were smaller than plots with a developed
319 canopy, as expected. One exception was at EF where the clear-cut plot exhibited the highest I_a of
320 the six EF plots (8.4%, Table 1). Notably, differences among EF plots were very small (I_a ranged
321 only from 7.9 to 8.4 % of annual rainfall), an annual interception rate consistent with or even
322 slightly lower than other clear cuts across the study. This site is extremely well drained and has
323 dense litter dominated by mosses and nutrient-poor sandy soils, highlighting the potential for
324 additional local measurements to better understand how forest structure controls observed
325 interception.

326 There are several important methodological considerations and assumptions inherent to
327 estimating interception using near-surface soil moisture data. First is the depth at which SMC is
328 measured. Ideally, soil moisture would be measured a few centimeters into the soil profile,
329 eliminating the need to account for infiltration when calculating P_G in Eqs. (4-6). Soil moisture
330 data used here were leveraged from a study of forest water yield, with sensor deployment depths
331 selected to efficiently integrate soil moisture patterns through the vadose zone. While the extra
332 step of modeling infiltration may increase uncertainty in β_s , infiltration was extremely well-
333 described using wetting front simulations of arrival time based on initial soil moisture and
334 rainfall. As such, while we advocate for shallower sensors in future efforts, our solution here
335 given the depths that were available seem tenable for this and other similar data sets. Second, in
336 contrast to the original Gash (1979) formulation, Eq. 5 does not explicitly include throughfall.
337 While throughfall has been a critical consideration for rainfall partitioning by the forest canopy,
338 our approach considers total interception by aboveground forest structures (canopy, groundcover,
339 and litter). A portion of canopy throughfall is captured by non-canopy storage and thus
340 intercepted. Constraining this fraction is not possible with the data available, and indeed our soil



341 moisture response reflects the “throughfall” passing the canopy, understory and litter. Similarly,
342 estimation of β_s using Eqs. 1-7 cannot directly account for stemflow, which can be an important
343 component of rainfall partitioning in forests (e.g., Bryant et al., 2005). We used the mean soil
344 moisture response across three sensor locations (close to a tree, away from the tree but below the
345 canopy, and within inter-canopy rows), which lessens the impact of this assumption on our
346 estimates of β_s . Finally, Eqs. (3-10) assume the same evaporation rate, E , for intercepted water
347 from the canopy and from the understory. Evaporation rates may vary substantially between the
348 canopy, understory, and forest floor [Gerrits et al., 2007, 2010], especially in more energy-
349 limited environments. Future work should consider differential evaporation rates within each
350 interception storage, particularly since the inclusion of litter as a component potentially
351 accentuates these contrasts in E .

352 Rainfall interception by forests is a dynamic process that is strongly influenced by
353 rainfall patterns (e.g., frequency, intensity), along with various forest structural attributes such as
354 interception storage capacity (β_s) [Gerrits et al., 2010]. In this work, we coupled estimation of a
355 total (or “whole-forest”) β_s parameter with a continuous water balance model [Liu, 1997, 2001;
356 Rutter et al., 1975], providing an integrative approach for quantifying time-varying and
357 cumulative interception losses. We propose that soil moisture-based estimates of β_s have the
358 potential to more easily and appropriately represent combined forest interception relative to
359 existing time- and labor-intensive field methods that fail to account for groundcover and litter
360 interception. Soil moisture can be measured relatively inexpensively and easily using continuous
361 logging sensors that require little field maintenance, facilitating application of the presented
362 approach across large spatial and temporal extents and reducing the time and resources that are
363 needed for other empirical measures [e.g., Lundberg et al., 1997]. Finally, while direct



364 comparisons with other empirical measures of forest canopy interception should be treated
365 cautiously, this approach yields values that are broadly consistent with the literature, and provide
366 an estimate of combined canopy and groundcover storage capacity that has the potential to
367 improve the accuracy of water balances models at scales from the soil column to watershed.

368

369

References

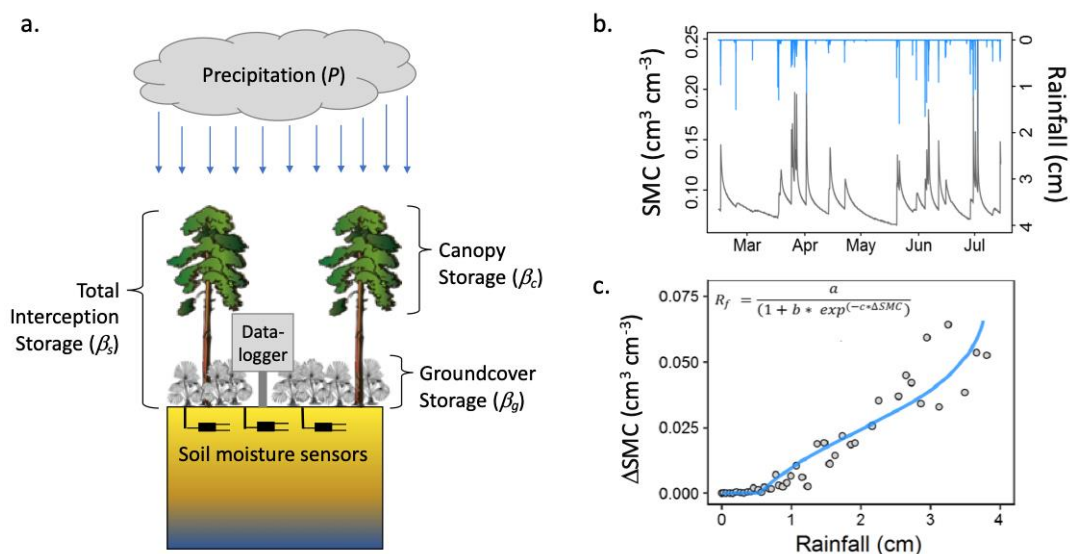
- 370 Acharya, B.S., Stebler, E., and Zou, C.B.: Monitoring litter interception of rainfall using leaf
371 wetness sensor under controlled and field conditions. *Hydrological Processes*, 31, 240-
372 249: DOI 10.1002/hyp.11047, 2005
- 373 Benyon, R.G., Doody, and T. M.: Comparison of interception, forest floor evaporation and
374 transpiration in *Pinus radiata* and *Eucalyptus globulus* plantations. *Hydrological*
375 *Processes* **29** (6): 1173–1187 DOI: 10.1002/hyp.10237, 2015
- 376 Bryant, M.L., Bhat, S., and Jacobs, J.M.: Measurements and modeling of throughfall variability
377 for five forest communities in the southeastern US. *Journal of Hydrology*, DOI:
378 10.1016/j.jhydrol.2005.02.012, 2005
- 379 Bulcock, H.H., and Jewitt, G.P.W.: Modelling canopy and litter interception in commercial
380 forest plantations in South Africa using the Variable Storage Gash model and idealised
381 drying curves. *Hydrol. Earth Syst. Sci* **16**: 4693–4705 DOI: 10.5194/hess-16-4693-2012,
382 2012
- 383 Carlyle-Moses, D.E., and Price, A.G.: Modelling canopy interception loss from a Mediterranean
384 pine-oak stand, northeastern Mexico. *Hydrological Processes* **21** (19): 2572–2580 DOI:
385 10.1002/hyp.6790, 2007
- 386 Carlyle-Moses, D.E., and Gash, J.H.C.: Rainfall Interception Loss by Forest Canopies. In
387 Carlyle-Moses and Tanaka (Eds), *Ecological Studies* 216. DOI: 10.1007/978-94-007-
388 1363, 2011
- 389 Crockford, R.H., and Richardson, D.P.: Partitioning of rainfall into throughfall, stemflow and
390 interception: effect of forest type, ground cover and climate. *Hydrological Processes* **14**
391 (16–17): 2903–2920 DOI: 10.1002/1099-1085(200011/12)14:16/17<2903::AID-
392 HYP126>3.0.CO;2-6, 2000
- 393 Gash, J.H.C., Lloyd, C.R., and Lachaud, B. G.: Estimating sparse forest rainfall interception with
394 an analytical model. *Journal of Hydrology* **170**: 79–86, 1995
- 395 Gash, J.H.C.: An analytical model of rainfall interception by forests. *Quarterly Journal of the*
396 *Royal Meteorological Society* **105** (443): 43–55 DOI: 10.1002/qj.49710544304, 1979



- 397 Gerrits, A.M.J., Savenije, H.H.G., Hofmann, L., and Pfister, L.: New technique to measure forest
398 floor interception – an application in a beech forest in Luxembourg. *Hydrol. Earth Syst.*
399 *Sci* **11**: 695–701, 2007
- 400 Ghimire, C.P., Bruijnzeel, L.A., Lubczynski, M.W., and Bonell, M.: Rainfall interception by
401 natural and planted forests in the Middle Mountains of Central Nepal. *Journal of*
402 *Hydrology* **475**: 270–280 DOI: 10.1016/j.jhydrol.2012.09.051, 2012
- 403 Ghimire, C.P., Bruijnzell, L.A., Lubczynski, M.W., Ravelona, M., Zwartendijk, B.W., and
404 Meervald, H.H.: Measurement and modeling of rainfall interception by two differently
405 aged secondary forests in upland eastern Madagascar, *Journal of Hydrology*, DOI:
406 10.1016/j.jhydrol.2016.10.032, 2017
- 407 Liu, J.: A theoretical model of the process of rainfall interception in forest canopy. *Ecological*
408 *Modelling* **42**: 111–123, 1988
- 409 Kelliher, F.M., Whitehead, D., and Pollock D.S.: Rainfall interception by trees and slash in a
410 young *Pinus radiata* D. Don stand. *Journal of Hydrology* **131** (1–4): 187–204 DOI:
411 10.1016/0022-1694(92)90217-J, 1992
- 412 Li, X., Xiao, Q., Niu, J., Dymond, S., Mcherson, E. G., van Doorn, N., Yu, X., Xie, B., Zhang,
413 K., and Li, J.: Rainfall interception by tree crown and leaf litter: an interactive process.
414 *Hydrological Processes* DOI: 10.1002/hyp.11275, 2017
- 415 Liu, S.: Evaluation of the Liu model for predicting rainfall interception in forests world-wide.
416 *Hydrological Processes* **15** (12): 2341–2360 DOI: 10.1002/hyp.264, 2001
- 417 Liu, S.: A new model for the prediction of rainfall interception in forest canopies. *Ecological*
418 *Modelling* **99**: 15–159, 2001
- 419 Liu, S.: Estimation of rainfall storage capacity in the canopies of cypress wetlands and slash pine
420 uplands in North-Central Florida. *Journal of Hydrology* **207**: 32–41, 1998
- 421 Llorens, P., and Poch, R.: Rainfall interception by a *Pinus sylvestris* forest patch overgrown in a
422 Mediterranean mountainous abandoned area I. Monitoring design and results down to
423 the event scale. *Journal of Hydrology* **199**: 331–345, 1997
- 424 Lundberg, A., Eriksson, M., Halldin, S., Kellner, E., and Seibert, J.: New approach to the
425 measurement of interception evaporation. *Journal of Atmospheric and Oceanic*
426 *Technology* **14** (5), 1023–1035, 1997
- 427 Massman, W.J.: The derivation and validation of a new model for the interception of rainfall by
428 forests. *Agricultural and Forest Meteorology* **28**: 261–286, 1983
- 429 Merriam, R.A.: A note on the interception loss equation. *Journal of Geophysical Research* **65**
430 (11): 3850–3851 DOI 10.1029/JZ065i011p03850, 1960

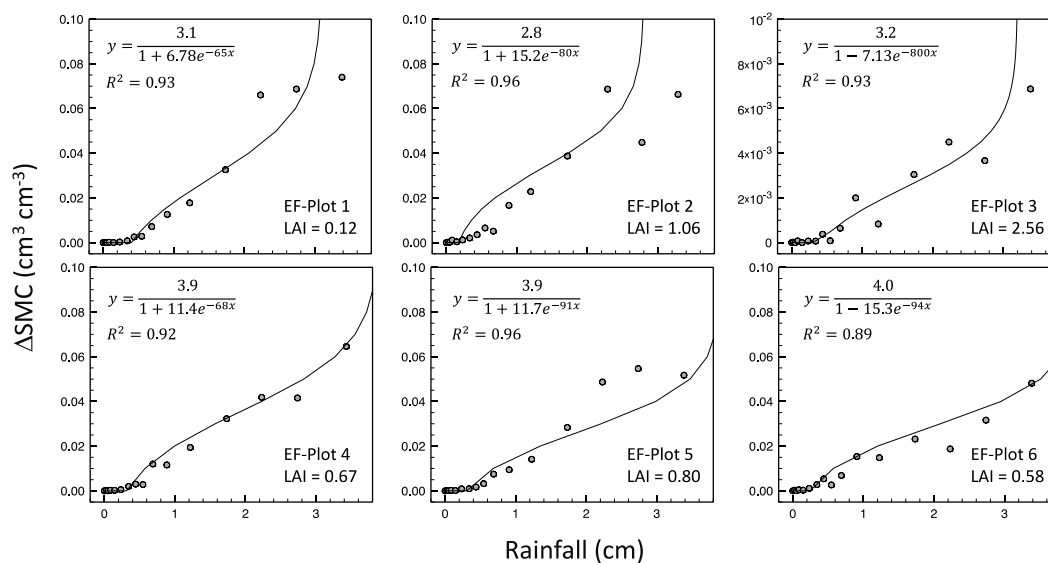


- 431 Muzylo, A., Llorens, P., Valente, F., Keizer, J.J., Domingo, F., and Gash, J.H.C. Gash. A review
432 of rainfall interception modelling. *Journal of Hydrology* **370**: 191–206 DOI:
433 10.1016/j.jhydrol.2009.02.058, 2009
- 434 Pook, E.W., Moore, P.H.R., and Hall, T.: Rainfall interception by trees of *Pinus radiata* and
435 *Eucalyptus viminalis* in a 1300 mm rainfall area of southeastern New South Wales: I.
436 Gross losses and their variability. *Hydrological Processes* **5** (2): 127–141 DOI:
437 10.1002/hyp.3360050202, 1991
- 438 Putuhena, W.M., and Cordery, I.: Estimation of interception capacity of the forest floor. *Journal*
439 *of Hydrology* **180**: 283–299, 1996
- 440 Rutter, A.J., Morton, A.J., and Robins, P.C.: A Predictive Model of Rainfall Interception in
441 Forests. II. Generalization of the Model and Comparison with Observations in Some
442 Coniferous and Hardwood Stands *Journal of Applied Ecology* **12** (1): 367–380, 1975
- 443 Savenije, H. H. G.: The importance of interception and why we should delete the term
444 evapotranspiration from our vocabulary, *Hydrol. Processes*, 18, 1507 – 1511, 2004
- 445 Schaap, M.G., Bouten, W., and Verstraten, J.M.: Forest floor water content dynamics in a
446 Douglas fir stand. *Journal of Hydrology* **201**: 367–383, 1997
- 447 Valente, F., David, J.S., and Gash, J.H.C.: Modelling interception loss for two sparse eucalypt
448 and pine forests in central Portugal using reformulated Rutter and Gash analytical
449 models. *Journal of Hydrology ELSEVIER Journal of Hydrology* **190**: 141–162, 1997
- 450 Van Dijk, A.I.J.M., and Bruijnzeel, L.A.: Modelling rainfall interception by vegetation of
451 variable density using an adapted analytical model. Part 1. Model description. *Journal of*
452 *Hydrology*, 247:230-238, 2001
- 453 Wei, Z., Yoshimura, K., Wang, L., Miralles, D.G., Jasechko, S., and Lee, X.: Revisiting the
454 contribution of transpiration to global terrestrial evapotranspiration. *Geophysical*
455 *Research Letters* **44** (6): 2792–2801 DOI: 10.1002/2016GL072235, 2017
- 456 Xiao, Q., McPherson, E.G., Ustin, S.L., and Grismer, M.E.: A new approach to modeling tree
457 rainfall interception. *Journal of Geophysical Research: Atmospheres* **105** (D23): 29173–
458 29188 DOI: 10.1029/2000JD900343, 2000
- 459



460

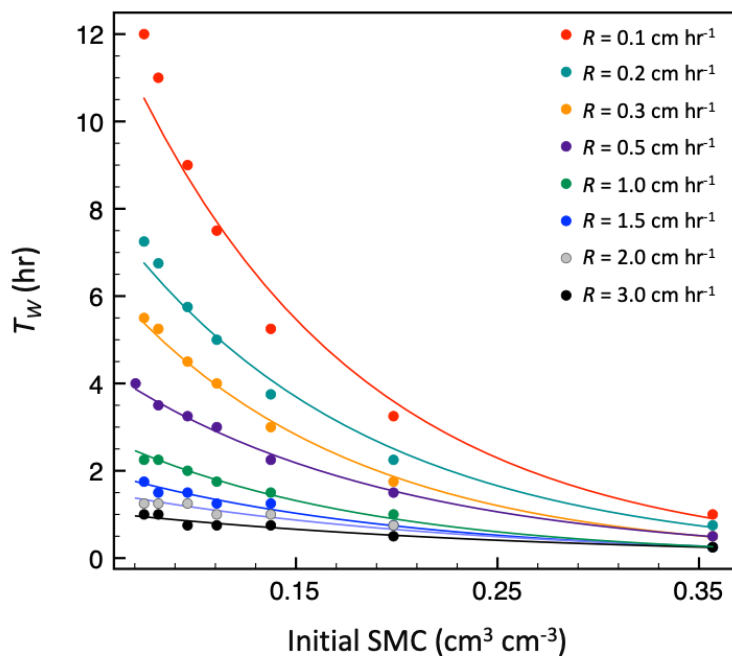
461 Figure 1. (a) Schematic illustration of experimental setup and interception water storages, where
 462 total interception storage (β_s) is the sum of canopy storage (β_c) and groundcover (understory and
 463 litter) storage (β_g). (b) Example time series of rainfall (blue lines) and corresponding near-
 464 surface soil moisture content (SMC , black line; observed at 15 cm in this study). (c) Resultant
 465 relationship between rainfall and change in soil moisture ΔSMC during rainfall, along with fitted
 466 model to extract the x-intercept (i.e., P_s).



467

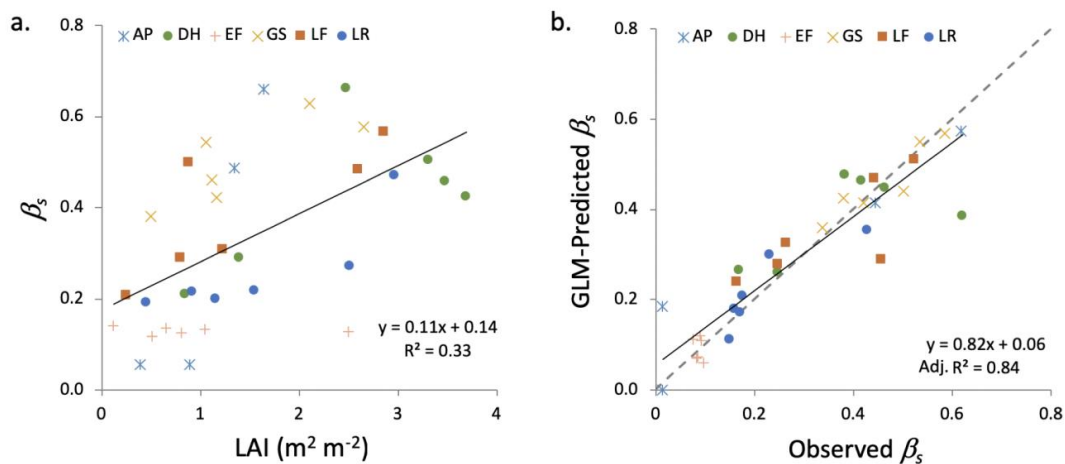
468 Figure 2: Change in soil moisture content (ΔSMC) versus binned rainfall depths for six plots at
 469 one of the study sites used in the study (Econfina; EF). The x-intercept of the fitted relationships
 470 were used to derive P_s in Eq. 2. Note different y-axis scale for EF-Plot 3.

471



472

473 Figure 3: Initial soil moisture content (SMC) versus time of wetting front arrival (T_w) for a loamy
474 sand soil. Dots are simulated results from HYDUS-1D simulation, and lines are the exponential
475 model given in Eq. 8, fitted for each rainfall rate, R .



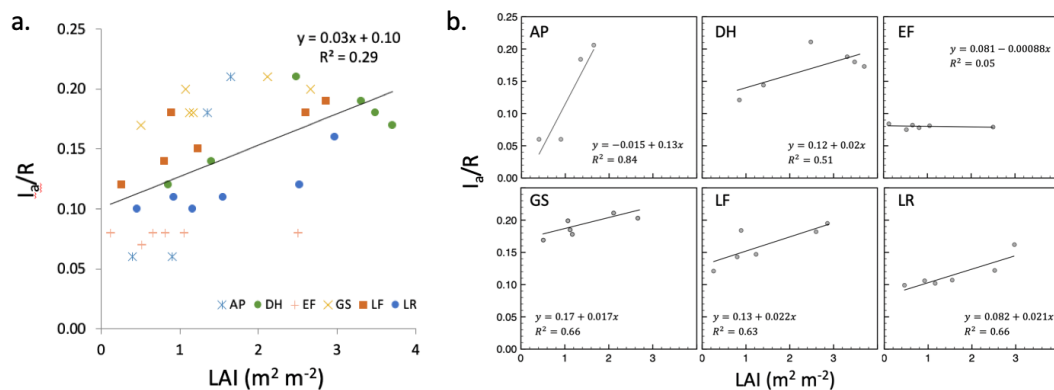
476

477 Figure 4. (a) Interception storage capacity (β_s) versus leaf area index (LAI) for all sites and plots.

478 (b) Modeled versus observed β_s using the best GLM, which included % groundcover vegetation

479 and an interaction term between site and LAI. The dashed line is the 1:1 line.

480



481

482

483

Figure 5. (a) Annual proportion of rainfall that is intercepted (I_a/R) intercepted versus LAI for all

484

sites and plots. (b) Site-specific I_a/R versus LAI relationships. The relationship is generally

485

strong except for the EF site, where the overall storage capacity is small across all values of LAI.

486



487 Table 1. Summary of storage capacity (β_s) and annual interception losses (I_a) for all sites and
 488 plots, along with plot characteristics (mean annual precipitation, P ; leaf area index, LAI; percent
 489 groundcover, %GC; and species). Note that the AP site only had three plots with the data
 490 required for the analysis.

Site	Plot	LAI	%GC	Species	β_s (cm)	R^2 ($\Delta SMC-R$)	P (cm)	I_a/P
AP	2	1.65	47.6	SF Slash	0.620	0.31	145.0	0.206
AP	3	0.90	62.8	SF Slash	0.014	0.78	145.0	0.06
AP	4	1.35	49.1	SF Slash	0.445	0.67	145.0	0.184
AP	6	0.40	73.4	Longleaf	0.014	0.57	145.0	0.06
DH	1	0.85	86.2	Loblolly	0.170	0.90	131.5	0.121
DH	2	2.48	51.2	Slash	0.621	0.68	131.5	0.211
DH	3	1.40	39.2	Slash	0.249	0.49	131.5	0.144
DH	4	3.31	35.8	Slash	0.464	0.71	131.5	0.188
DH	5	3.70	27.1	Loblolly	0.383	0.69	131.5	0.173
DH	6	3.48	32.9	Slash	0.418	0.40	131.5	0.18
EF	1	0.12	13.6	Clearcut	0.099	0.93	153.8	0.084
EF	2	1.05	56.9	Slash	0.092	0.96	153.8	0.081
EF	3	2.50	11.8	Sand	0.086	0.93	153.8	0.079
EF	4	0.66	50.9	Slash	0.094	0.92	153.8	0.082
EF	5	0.81	17.9	Sand	0.085	0.96	153.8	0.078
EF	6	0.52	52.0	Longleaf	0.076	0.89	153.8	0.075
GS	1	1.07	67.9	Clearcut	0.502	0.84	132.4	0.199
GS	2	2.66	7.9	Slash	0.535	0.88	132.4	0.203
GS	3	2.11	71.5	Slash	0.587	0.82	132.4	0.211
GS	4	1.12	42.4	Slash	0.421	0.90	132.4	0.185
GS	5	1.17	45.6	Slash	0.382	0.76	132.4	0.178
GS	6	0.51	55.2	Longleaf	0.339	0.78	132.4	0.169
LF	1	0.26	43.5	None	0.166	0.85	136.3	0.121
LF	2	2.86	23.1	Slash	0.525	0.64	136.3	0.195
LF	3	1.23	24.9	Slash	0.266	0.72	136.3	0.147
LF	4	0.80	25.7	Slash	0.248	0.64	136.3	0.143
LF	5	2.60	12.3	Slash	0.443	0.63	136.3	0.182
LF	6	0.89	25.9	Longleaf	0.458	0.69	136.3	0.184
LR	1	0.46	34.0	Clearcut	0.151	0.96	144.5	0.099
LR	2	2.97	38.1	Slash	0.429	0.84	144.5	0.162
LR	3	0.92	47.0	Slash	0.173	0.95	144.5	0.106
LR	4	2.52	26.7	Slash	0.232	0.92	144.5	0.122
LR	5	1.55	28.1	Slash	0.177	0.96	144.5	0.107
LR	6	1.16	35.5	Longleaf	0.160	0.96	144.5	0.102

491



492 Table 2. Summary of generalized linear model (GLM) results for interception storage capacity
493 (β_s). LAI is leaf area index, GC is groundcover, and WT is water table (shallow vs. deep). The
494 best model (by AIC) is shown in bold.

Model #	Variable(s)	AIC	R ²
1	LAI	378.1	0.32
2	LAI + site	318.5	0.66
3	LAI * site	255.9	0.83
4	LAI * site + GC	253.1	0.84
5	LAI + WT	338.3	0.55
6	LAI * WT	339.8	0.55
7	LAI * WT + GC	341.8	0.55
8	LAI + WT + GC	340.3	0.55

495